

Effective Temperature in an Interacting Vertex System: Theory and Experiment on Artificial Spin Ice

Cristiano Nisoli,¹ Jie Li,² Xianglin Ke,² D. Garand,² Peter Schiffer,² and Vincent H. Crespi²

¹Theoretical Division and Center for Nonlinear Studies, Los Alamos National Laboratory, Los Alamos, New Mexico 87545, USA

²Department of Physics and Materials Research Institute, 104 Davey Lab, Pennsylvania State University, University Park, Pennsylvania 16802, USA

(Received 16 December 2009; published 23 July 2010)

Frustrated arrays of interacting single-domain nanomagnets provide important model systems for statistical mechanics, as they map closely onto well-studied vertex models and are amenable to direct imaging and custom engineering. Although these systems are manifestly athermal, we demonstrate that an effective temperature, controlled by an external magnetic drive, describes their microstates and therefore their full statistical properties.

DOI: 10.1103/PhysRevLett.105.047205

PACS numbers: 75.50.Lk, 75.10.Jm, 75.25.-j, 75.75.-c

The physical meaning of temperature can be approached on several distinct levels. Operatively and macroscopically, one appeals to the notion of thermal equilibrium. More formally, temperature measures the variation of energy with disorder. In statistical mechanics, temperature emerges as the Lagrange multiplier in an energy-constrained optimization. Traditionally, a “thermal” system at equilibrium supports all three of these notions. Yet the concept of temperature has been extended to athermal systems, such as driven granular materials where the characteristic interaction energies greatly exceed the standard thermodynamic temperature [1–3] (often in the context of glassy transitions, jamming, and rheology [4–7]) on the grounds that the large number of grains would still warrant statistical descriptions [8]. Effective temperatures have thus been introduced theoretically [9], extracted from simulations of slowly sheared granular matter [10], and from experiments of Brownian motion in vibrofluidized grains, in which it increases with the magnitude of the vibratory external drive [11].

While these seminal results reflect the granular kinetics of systems interacting only through hard-core repulsion and possibly friction, in this Letter we demonstrate that an *energy-based* effective temperature can be defined, extracted, and used to make predictions, in a recently introduced nanometer-scale metamaterial, “artificial spin ice” [12–17], which is controlled by nontrivial interactions, can be engineered to replicate complex models of statistical mechanics [18–20], and whose microstates can be directly imaged.

Our artificial spin ice system is a two-dimensional array of elongated single-domain permalloy islands ($80 \times 220 \times 25 \text{ nm}^3$, with a magnetic moment $\sim 10^7 \mu_B$) whose shape anisotropy defines Ising-like spins arranged along the sides of a regular lattice. The microstate of island moments in this system can be directly imaged via magnetic force microscopy (MFM) [12,13,21], in contrast to the naturally occurring magnetically frustrated materials

such as the spin ice pyrochlores [22–25]. The system is athermal: The magnetostatic interaction and anisotropy energies of the islands are $\sim 10^5 \text{ K}$, and thus thermal excitations cannot induce spin flips. However, as for granular systems, the large number of islands suggests the viability of statistical treatments, if activated by an external drive. Artificial spin ice can be driven into a low-energy, interaction-dominated state [12,13,21,26,27] by rotating the sample in a decreasing magnetic field. In our experiments, the field decreases from 2000 Oe (far above coercive field) to 0 in steps of H_s , holding each step for 5 seconds while the sample rotates at 1000 rpm, with a reversal of field direction at each step. This demagnetization protocol was implemented for a range of field step sizes (H_s) and for two lattice geometries, square ice and hexagonal ice, as depicted in Fig. 1, of different lattice constants.

The dominant interactions in the lattice occur between neighboring islands across a given vertex. Hence we follow a previously established approach [12,27,28] and describe the data within a vertex model [20] thus considering populations of distinct vertex types, each with a given magnetostatic energy. Square ice has 4 topologically distinct vertex types, which we call types I, II, III, and IV, with multiplicities $q_I = 2$, $q_{II} = 4$, $q_{III} = 8$, and $q_{IV} = 2$ as defined in Fig. 1. We call the magnetostatic self-energies of these vertices E_I , E_{II} , E_{III} , and E_{IV} with fractional populations n_I , n_{II} , n_{III} , and n_{IV} ; these can be extracted from MFM images. The specific vertex energy is then simply $\bar{E} = E_I n_I + E_{II} n_{II} + E_{III} n_{III} + E_{IV} n_{IV}$. Hexagonal ice has just two vertex topologies of multiplicity $q_I = 6$ and $q_{II} = 2$ with specific vertex energy $\bar{E} = E_I n_I + E_{II} n_{II}$. The two lattice geometries have very different entropy vs energy curves within the vertex model: Square ice has a twofold ground state of antiferromagnetically tiled type-I vertices, whereas hexagonal ice has an extensively degenerate ground-state tiling of type-I vertices with a substantial residual entropy. Not surprisingly, they behave

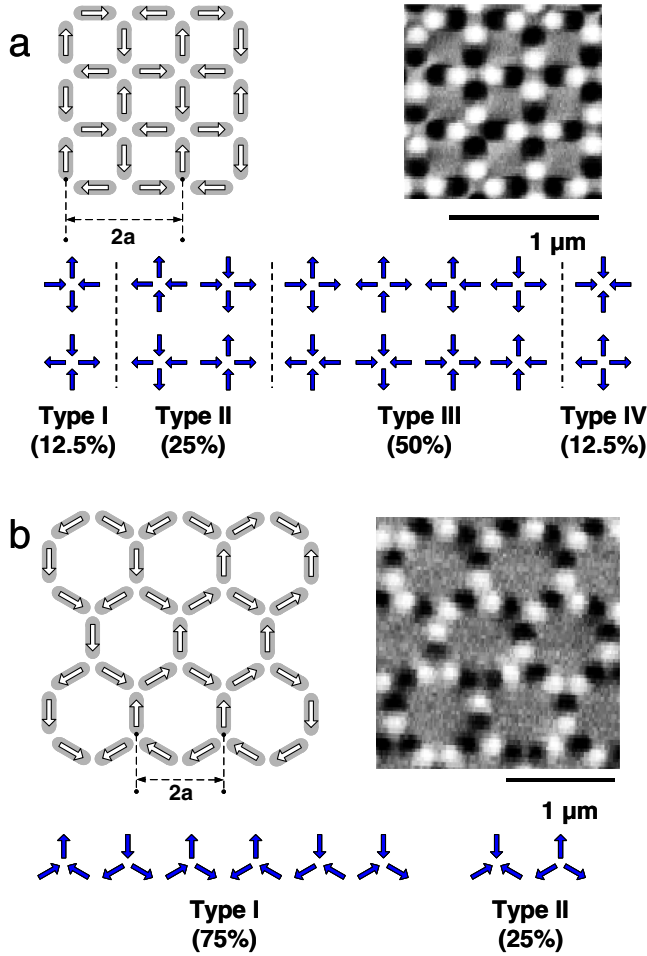


FIG. 1 (color online). Square and hexagonal artificial spin ice. (a) Schematics (top left) and MFM (top right) of the square arrays and the 16 vertices of the square artificial ice (bottom). (b) Schematics (top left) and MFM (top right) of the hexagonal arrays with the 8 vertices of the hexagonal. White arrows show the vertex ground states, and the percentages indicate the vertex multiplicity.

differently under ac demagnetization: Square ice never finds (or closely approaches) the ground state, whereas demagnetized hexagonal ice returns the vertex-model ground state with at most sparse excitations.

We first consider the case of the square ice arrays, with lattice constant $a = 400, 440, 480, 560, 680,$ and 880 nm. The external field in our rotational demagnetization is initially strong enough to coerce every island into following the external field, but, as its magnitude decreases, successive islands presumably begin to “fall away” from the field, locked in by favorable magnetostatic interactions with their neighbors. The accumulation of these distinct “defects” carved in the initial uniform set of aligned type-II vertices generates a well-defined statistical system. In an isotropic, vertex-gas approximation, where each vertex is treated as an independent entity, there are $M = \frac{N!}{(N-D)! \prod_{\alpha} \frac{q_{\alpha}^{N_{\alpha}}}{N_{\alpha}!}}$ ways to choose D defected vertices among

the N vertices of a given lattice, each allocated among the four degenerate vertex types according to a distribution N_{α} of degeneracy q_{α} , $\alpha = \text{I}, \dots, \text{IV}$. Calling $\rho = D/N$ and $v_{\alpha} = N_{\alpha}/D$, we consider $S = \ln M$ and maximize it under a vertex-energy constraint on the ensemble of defected vertices, or $\rho\sigma - \rho \ln \rho - (1 - \rho) \ln(1 - \rho) - \rho \beta_e (\sum_{\alpha=1}^{\text{IV}} E_{\alpha} v_{\alpha} - E)$, where $\sigma = -\sum_{\alpha=1}^{\text{IV}} v_{\alpha} \ln \frac{v_{\alpha}}{q_{\alpha}}$ is the “entropy” of the defected ensemble. We obtain a canonical distribution for the defects

$$v_{\alpha} = \frac{q_{\alpha} \exp(-\beta_e E_{\alpha})}{Z(\beta_e)} \quad (1)$$

[$Z(\beta_e)$ is defined by normalization of v_{α}] as well as an expression for the auxiliary quantity ρ

$$\rho(\beta_e) = \frac{1}{\exp[-\sigma(\beta_e)] + 1}, \quad (2)$$

where $\sigma(\beta_e)$ is obtained by substitution of Eq. (1) into the expression for σ . Equations (1) and (2) provide the relative v_{α} vertex population densities as

$$\begin{aligned} n_{\text{I}} &= \rho v_{\text{I}}, & n_{\text{III}} &= \rho v_{\text{III}}, & n_{\text{IV}} &= \rho v_{\text{IV}}, \\ n_{\text{II}} &= (1 - \rho) + \rho v_{\text{II}}. \end{aligned} \quad (3)$$

We compute the vertex energies by using a “dumbbell” model (as in Ref. [29]), in which the magnetic dipole is treated as a finite-size dumbbell of monopoles, and we consider only interactions between monopoles converging in each vertex: Energies then scale as $(a - l)^{-1}$ (where a is the lattice constant and l the length of the islands). By imposing $E_{\text{I}} = 0$ and $E_{\text{III}} = 1$, one finds $E_{\text{II}} = (\sqrt{2} - 1)/(\sqrt{2} - 1/2)$ and $E_{\text{IV}} = 4\sqrt{2}/(2\sqrt{2} - 1)$. In this simple dumbbell model of the energetics, the ratios between different vertex energies are independent of the array lattice constant.

As a simple test of the basic assumptions of the model above [1], we consider the quantities $\ln(5n_{\text{I}}/2n_{\text{II}})$ and $\ln(8n_{\text{I}}/2n_{\text{III}})$ as deduced from the measured n_{I} , n_{II} , and n_{III} . These quantities should be proportional to the reciprocal effective temperatures $E_{\text{II}}\beta_e$ and $E_{\text{III}}\beta_e$, since our predictions for the vertex populations [Eq. (3)] at high temperatures are well approximated by a purely canonical distribution that assigns an anomalous multiplicity of 5 rather than 4 to type-II vertices—a fact that can be checked by direct calculation but which also seems reasonable as there are four different multiplicities in the defected sample and one in the background. In Fig. 2, we plot these two quantities against each other. A linear fit returns $E_{\text{II}}/E_{\text{III}} = 0.441$, very close to the expected theoretical value $E_{\text{II}}/E_{\text{III}} = (\sqrt{2} - 1)/(\sqrt{2} - 1/2) = 0.453$ obtained from the dumbbell approximation.

In Fig. 3(a), we plot the experimentally observed populations of each vertex type vs the effective reciprocal temperature extracted from $\beta_e E_{\text{III}} = \ln \frac{4n_{\text{I}}}{n_{\text{III}}}$ and the theoretical curves for the vertex populations as a function of the

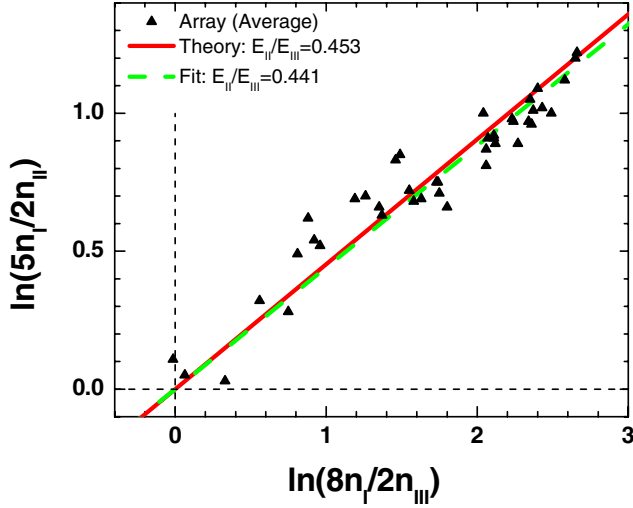


FIG. 2 (color online). The effective temperature of the square arrays, plotted as $\ln(5n_I/2n_{II})$ vs $\ln(8n_I/2n_{III})$: The linear fit returns a ratio very close to the theoretical value. (n_I , n_{II} , and n_{III} are average values from the MFM images taken on the same array and at same magnetic step size.)

effective temperatures, based on Eqs. (1)–(3). The excellent agreement between theory and the experimental data demonstrates the predictive power of the effective temperature.

Is the effective temperature derived above only a Lagrange multiplier, or does it provide physical information about the “fluidizing” external magnetic drive, as an actual physical temperature provides information about the surrounding thermodynamic bath? We found that effective temperature can be controlled via the external drive in a way strikingly analogous to that reported for vibrofluidized granular materials [11]—but here in a system with an explicit *energetic* description of interactions. As seen in Fig. 3(b), we find a strikingly linear dependence of $\langle\beta_e\rangle$ in the magnetic step size of the ac demagnetization, indicating that the effective temperature description does indeed have a physical basis akin to actual temperature.

We now consider the effective temperature of the hexagonal ice arrays, in which ac demagnetization consistently returns the vertex ground state (all type-I vertices) for arrays of small lattice constant. For $a = 225, 260, 320,$ and 425 nm, the frequency of excitations is $\sim 10^{-3}$, below experimental error. Hence hexagonal ice is a good candidate to study effective temperature only for larger lattice constants $a = 650, 910, 1135, 1395,$ and 1620 nm, wherein the occurrence of excitations n_{II} is significant. As the density of excitations n_{II} completely defines the thermodynamics, the introduction of an effective temperature as for the square ice, $\beta_e E_{II} = \ln(n_I/3n_{II})$, might seem only a reparametrization with little predictive power. In Fig. 4(a), however, we extract $\ln(n_I/n_{II})$ from arrays of different lattice constant a , but annealed with the same magnetic step H_s , and plot that ratio against the respective energy

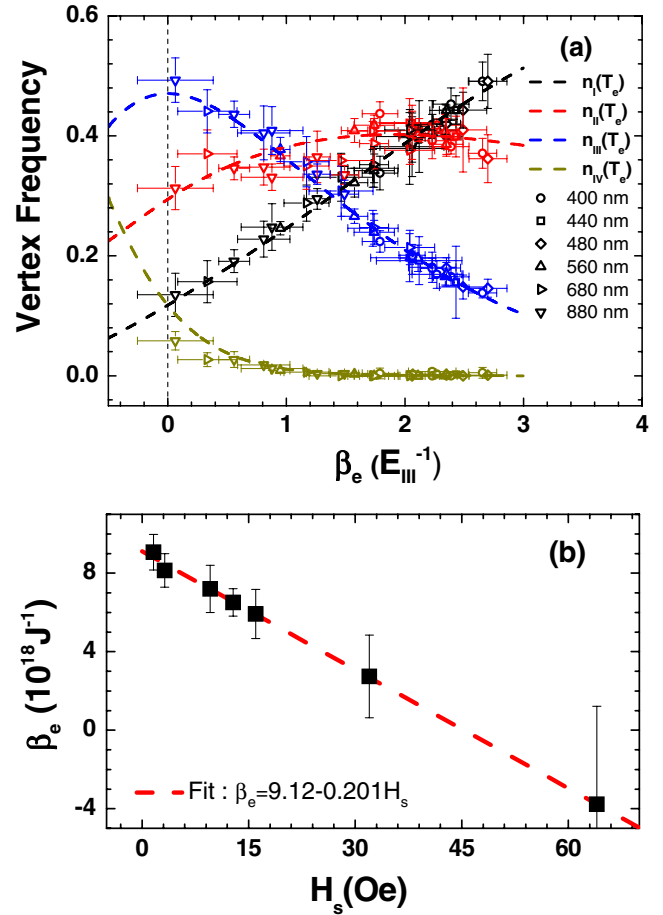


FIG. 3 (color online). (a) Vertex frequency from square arrays of different lattice constants and H_s , plotted against their effective reciprocal temperature β_e in units of E_{III}^{-1} . Data are from averaging at least three MFM images from the same array with the same H_s . Lines are theoretical curves from Eqs. (1)–(3). (b) Linear dependence between β_e and the magnetic step size H_s (data are averaged over the lattice constant a). Negative temperatures are possible, because of high-energy, low-entropy states.

E_{II} . Somewhat surprisingly, we find a linear behavior, which suggests an effective temperature that is independent of the lattice constant. In this calculation, the vertex energies are obtained via micromagnetic calculations that describe the full vertex interaction of dipole islands [30], since we now study much larger lattices for which the dumbbell approximation (which treats only the monopole tips that converge at a vertex) is less accurate. The intercept of the fits in Fig. 4(a) is surprisingly close to the expected $\ln(q_I/q_{II}) = \ln 3$, lending further credence to the analysis. The extracted effective temperature β_e is plotted in Fig. 4(b) against the magnetic step size H_s . As in the case of the square ice, we again find a remarkable linear dependence of β_e on the anneal step size H_s , although with different parameters (different geometries apparently experience different effective temperatures under the same

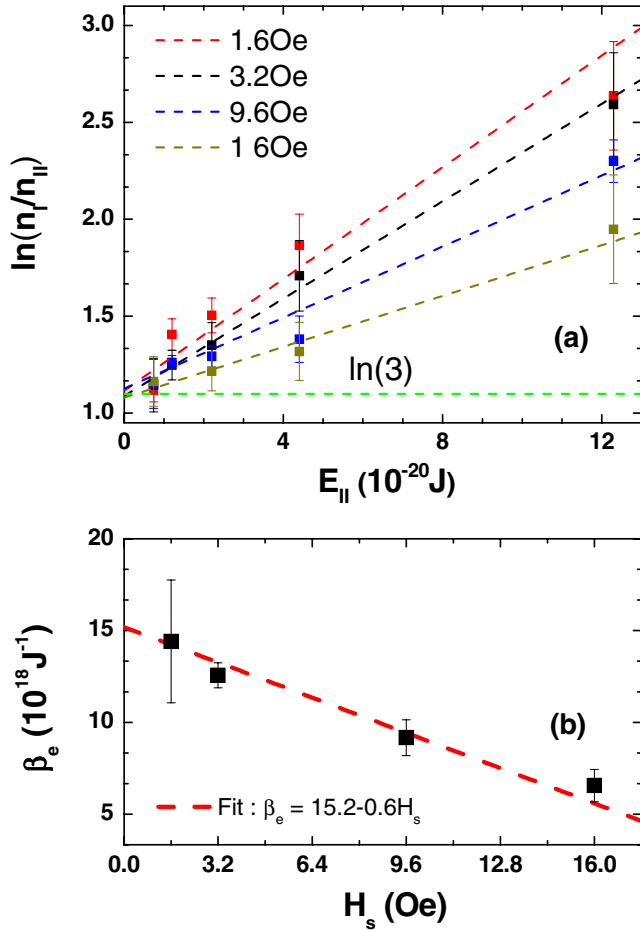


FIG. 4 (color online). (a) Linear fits of $\ln(n_{II}/n_I)$ for the hexagonal arrays vs the energy E_{II} , for the larger lattice spacing. The intercept falls very close to the expected multiplicity $q_I/q_{II} = 3$ [i.e., $\ln(3)$, since the graph plots the logarithm]. (b) Linear dependence of β_e as a function of the magnetic step size; β_e obtained from the fitting slope in (a).

magnetic drive). These results support the physical nature of the effective temperature, one that can be generalized to multiple geometries of artificial ice systems, although the reason for the linearity in H_s is not obvious.

In conclusion, we have introduced a predictive notion of effective temperature in a complex interacting system of magnetostatically interacting nanomagnets. We have found that the external drive, in the form of an agitating magnetic field, behaves as a thermal bath and controls the temperature. The formalism successfully predicts microstates on a wide spectrum of different energies and vertex populations. Unlike granular materials in which effective temperature has been previously explored, the nanomagnet arrays can be engineered to reproduce known models of

statistical mechanics, and the interactions can be controlled by design, suggesting that a range of other statistical physics may be accessed in these systems.

This work was supported by the Army Research Office and the National Science Foundation MRSEC program (DMR-0820404) and the National Nanotechnology Infrastructure Network. The work of C.N. was carried out under the auspices of the National Nuclear Security Administration of the U.S. Department of Energy at Los Alamos National Laboratory under Contract No. DE-AC52-06NA25396. We are grateful to Professor Chris Leighton and Dr. Mike Erickson for the film deposition.

- [1] D. Sornette, *Critical Phenomena in Natural Sciences* (Springer-Verlag, Heidelberg, 2004).
- [2] H. M. Jaeger *et al.*, *Rev. Mod. Phys.* **68**, 1259 (1996).
- [3] B. Behringer, *Nature (London)* **415**, 594 (2002).
- [4] A. R. Abate and D. J. Durian, *Phys. Rev. Lett.* **101**, 245701 (2008).
- [5] P. Sollich *et al.*, *Phys. Rev. Lett.* **78**, 2020 (1997).
- [6] V. Colizza *et al.*, *Phys. Rev. E* **65**, 050301 (2002).
- [7] C. M. Song *et al.*, *Proc. Natl. Acad. Sci. U.S.A.* **102**, 2299 (2005).
- [8] L. F. Cugliandolo *et al.*, *Phys. Rev. E* **55**, 3898 (1997).
- [9] A. Mehta *et al.*, *Physica (Amsterdam)* **157A**, 1091 (1989).
- [10] H. A. Makse and J. Kurchan, *Nature (London)* **415**, 614 (2002).
- [11] G. D'Anna *et al.*, *Nature (London)* **424**, 909 (2003).
- [12] R. F. Wang *et al.*, *Nature (London)* **439**, 303 (2006).
- [13] J. Li *et al.*, *Phys. Rev. B* **81**, 092406 (2010).
- [14] Q. Yi *et al.*, *Phys. Rev. B* **77**, 094418 (2008).
- [15] A. Westphalen *et al.*, *Phys. Rev. B* **77**, 174407 (2008).
- [16] M. Tanaka *et al.*, *Phys. Rev. B* **73**, 052411 (2006).
- [17] E. Mengotti *et al.*, *Phys. Rev. B* **78**, 144402 (2008).
- [18] E. H. Lieb, *Phys. Rev. Lett.* **18**, 1046 (1967).
- [19] E. H. Lieb and F. W. Wu, *Phase Transitions and Critical Phenomena* (Academic, London, 1971), Vol. 1.
- [20] R. Baxter, *Exactly Solved Models in Statistical Physics* (Academic, New York, 1982).
- [21] X. Ke *et al.*, *Phys. Rev. Lett.* **101**, 037205 (2008).
- [22] A. P. Ramirez, in *Handbook of Magnetic Materials* (Elsevier Science, Amsterdam, 2001).
- [23] R. Moessner, *Can. J. Phys.* **79**, 1283 (2001).
- [24] L. C. Pauling, *J. Am. Chem. Soc.* **57**, 2680 (1935).
- [25] S. T. Bramwell and M. J. P. Gingras, *Science* **294**, 1495 (2001).
- [26] R. F. Wang *et al.*, *J. Appl. Phys.* **101**, 09J104 (2007).
- [27] C. Nisoli *et al.*, *Phys. Rev. Lett.* **98**, 217203 (2007).
- [28] G. Möller, and R. Moessner, *Phys. Rev. Lett.* **96**, 237202 (2006).
- [29] C. Castelnovo *et al.*, *Nature (London)* **451**, 42 (2008).
- [30] OOMMF NIST code. <http://math.nist.gov/oommf> (2005).